HHS Public Access

Author manuscript

Hippocampus. Author manuscript; available in PMC 2019 November 29.

Published in final edited form as:

Hippocampus. 2017 November ; 27(11): 1125–1139. doi:10.1002/hipo.22757.

Hippocampal gamma-slow oscillation coupling in macaques during sedation and sleep

Andrew G. Richardson[1], **Xilin Liu**[2], **Pauline K. Weigand**[1], **Eric D. Hudgins**[1], **Joel M. Stein**[3], **Sandhitsu R. Das**[4], **Alexander Proekt**[5], **Max B. Kelz**[5], **Milin Zhang**[6], **Jan Van der Spiegel**[2], **Timothy H. Lucas**[1]

[1]Department of Neurosurgery, University of Pennsylvania, Philadelphia, PA, USA

[2]Department of Electrical and Systems Engineering, University of Pennsylvania, Philadelphia, PA, USA

[3]Department of Radiology, University of Pennsylvania, Philadelphia, PA, USA

[4]Department of Neurology, University of Pennsylvania, Philadelphia, PA, USA

[5]Department of Anesthesiology and Critical Care, University of Pennsylvania, Philadelphia, PA, USA

[6]Department of Electronic Engineering, Tsinghua University, Beijing, China

Abstract

Behavioral and neurophysiological evidence suggests that the slow (≤ 1 Hz) oscillation (SO) during sleep plays a role in consolidating hippocampal (HIPP)-dependent memories. The effects of the SO on HIPP activity have been studied in rodents and cats both during natural sleep and during anesthetic administration titrated to mimic sleep-like slow rhythms. In this study, we sought to document these effects in primates. First, HIPP field potentials were recorded during ketamine-dexmedetomidine sedation and during natural sleep in three rhesus macaques. Sedation produced regionally-specific slow and gamma (~40 Hz) oscillations with strong coupling between the SO phase and gamma amplitude. These same features were seen in slow-wave sleep (SWS), but the coupling was weaker and the coupled gamma oscillation had a higher frequency (~70 Hz) during SWS. Second, electrical stimuli were delivered to HIPP afferents in the parahippocampal gyrus (PHG) during sedation to assess the effects of sleep-like SO on excitability. Gamma bursts after the peak of SO cycles corresponded to periods of increased gain of monosynaptic connections between the PHG and HIPP. However, the two PHG-HIPP connectivity gains during sedation were both substantially lower than when the animal was awake. We conclude that the SO is correlated with rhythmic excitation and inhibition of the PHG-HIPP network, modulating connectivity and gamma generators intrinsic to this network. Ketamine-dexmedetomidine sedation produces a similar effect, but with a decreased contribution of the PHG to HIPP activity and gamma generation.

Corresponding author: Andrew G. Richardson, PhD, University of Pennsylvania, 502C Stemmler Hall, 3450 Hamilton Walk, Philadelphia, PA 19104, 215-746-4233, andrew.richardson@uphs.upenn.edu.

Keywords

monkey; neurophysiology; connectivity; ketamine; dexmedetomidine

Introduction

The slow (≤ 1 Hz) oscillation (SO) of non-rapid eye movement sleep is thought to play a critical role in the consolidation of newly-formed memories (Diekelmann and Born, 2010). There is substantial behavioral evidence linking the amount of SO activity after learning to the strength of both procedural and declarative memories (Huber et al., 2004; Marshall et al., 2006). The neurophysiological mechanisms governing the SO-memory relationship are beginning to be elucidated.

The SO reflects synchronous neuronal excitability changes that are widespread throughout the neocortex (Steriade et al., 1993b) and hippocampus (HIPP) (Wolansky et al., 2006). Through these coordinated excitability changes, the SO appears to facilitate interaction between the HIPP and neocortex for the purpose of memory storage. In particular, the SO synchronizes HIPP sharp-wave ripples (SWR) and thalamocortical spindles, two key sleep-related field potential oscillations (Siapas and Wilson, 1998; Battaglia et al., 2004; Molle et al., 2006; Staresina et al., 2015). In turn, this set of nested oscillations is hypothesized to provide the temporal structure for repeated reactivation, in both the HIPP and neocortex, of the pattern of HIPP neuronal activity that represents the new memory, thus strengthening and transferring the pattern via Hebbian plasticity (Kudrimoti et al., 1999; Csicsvari et al., 2000; Destexhe and Sejnowski, 2003; Ji and Wilson, 2007).

These neurophysiological properties of the SO have largely been studied in rodents and cats. Little is known of HIPP activity during the SO in primates. There is recent interest in clinical neuromodulation therapies to improve memory after medial temporal lobe injury or disease (Suthana and Fried, 2014). A better understanding of the SO in primates could inform such therapies. Two recent studies examined HIPP field potentials during natural sleep in monkeys (Tamura et al., 2013; Takeuchi et al., 2015). They found SO in the HIPP and cross-frequency coupling between the SO and gamma (30–90 Hz) oscillations. The gamma-SO relationship was similar to the ripple-SO (80–100 Hz) coupling seen in the HIPP of sleeping humans (Staresina et al., 2015). Due to limits in achievable interactions with sleeping monkeys and humans, these studies did not apply stimuli to probe HIPP excitability changes correlated with the SO.

To facilitate more detailed experiments and increase the duration of the transient SO, prior studies in rodents and cats have used anesthesia to induce sustained, sleep-like SO in the HIPP and cortex (Steriade et al., 1993b; Sharma et al., 2010; Chauvette et al., 2011). Among other agents, a cocktail of the NMDA-receptor antagonist ketamine and an α_2-adrenergic receptor agonist, such as xylazine or dexmedetomidine, can produce sleep-like SO in non-primates (Sharma et al., 2010; Zhang et al., 2012). However, the properties of natural and anesthesia-induced SO in cats did differ in some respects (Chauvette et al., 2011).

In this study, we sought to characterize SO in monkeys during both natural sleep and ketamine-dexmedetomidine sedation. We hypothesized that sleep-like SO in the HIPP could be induced with sedation. Also, based on the prior work in monkeys and humans, we hypothesized that a major feature of SO activity in both states would be cross-frequency coupling with gamma/ripple-frequency oscillations. Finally, we hypothesized that SO phase would modulate HIPP excitability, which we quantified by delivering electrical stimuli to HIPP afferents in the parahippocampal gyrus (PHG).

Materials and Methods

Three male rhesus macaques (*Macaca mulatta*), monkeys O, D, and F (8–12 kg), were used in this study. The procedures described below were approved by the Institutional Animal Care and Use Committee (IACUC) of the University of Pennsylvania and the Animal Care and Use Review Office (ACURO) of the Department of Defense.

Surgery and imaging

Preparation of each monkey for this study consisted of four steps, with a minimum of three weeks of recovery time between each step. First, a sterile surgery was performed to attach a post to the skull with screws and acrylic. The post provided a skull-fixed holder for an array of imaging fiducial markers. In monkey F, the post was also used for head fixation during awake sessions. Second, magnetic resonance (MR) images of the brain were acquired with fiducial markers securely attached to the post. Third, a second sterile surgery was performed to implant the electrode arrays. Three, clinical-grade electrode arrays (SD08R-AP58X-000, Ad-Tech Medical Instrument Corp) were implanted using a MR-guided neuronavigation system (Brainsight, Rogue Research Inc). The 8-electrode cylindrical arrays had 1.1-mm diameter, 2.2-mm interelectrode spacing, and 1.32-mm long platinum electrodes (Fig. 1A). A transoccipital approach, adapted from human procedures (Bekelis et al., 2013; Wu et al., 2014), was used to place one array each along the longitudinal axis of the HIPP and PHG of the left hemisphere. The third array targeted deep medial structures and was used only as a control for the purposes of this study. The connector tails of the arrays were housed in a custom plastic chamber secured to the skull anterior to the post with screws and acrylic. An uninsulated silver wire, which served as the reference electrode for neural recordings, was wrapped around the skull screws before applying acrylic. Fourth, after implantation, computed tomography (CT) images of the brain were acquired to permit identification of the anatomical location of each implanted electrode as described below.

Note that clinical macroelectrodes were used in this study, rather than more conventional microelectrodes, since the broader goals of the funded project were to identify closed-loop stimulation paradigms for modulating memory that would be immediately suitable for human patients. This prevented us from recording single neurons and isolating individual HIPP subfields with great confidence. However, as described in the Results, the field potential recordings were sufficiently localized to document regionally-specific, sleep-related oscillations and effective PHG-HIPP connectivity.

Electrode localization

Thin-section, post-implantation head CT images demonstrating the position of the radiodense electrode arrays were co-registered to pre-implantation, T1-weighted anatomic MR images using FMRIB's Linear Image Registration Tool (Jenkinson et al., 2002). MR images were additionally registered to the INIA19 Macaca mulatta template brain (Rohlfing et al., 2012) using Advanced Normalization Tools (Avants et al., 2008), allowing the electrode contacts from the CT to be overlaid on the NeuroMaps brain atlas (Fig. 1B). A neuroradiologist with expertise in medial temporal lobe anatomy confirmed the position of contacts within the HIPP and PHG on individual and template brain images.

Electrophysiology during sedation and sleep

Sedated sessions began with a single intramuscular injection of a ketamine (4 mg/kg) - dexmedetomidine (0.05 mg/kg) cocktail. The monkey was then transferred on a cart from his cage to a shielded recording booth. The cap of the head-fixed chamber was removed and the electrodes were connected to a commercial neurophysiology system (RZ2, Tucker-Davis Technologies). In 10 sedated sessions (monkey D = 5 sessions, F = 2, O = 3), spanning 3–8 weeks in each animal, we assessed sleep-like oscillatory activity during sedation by simultaneous recording from all electrodes for the duration of the session. The wide-band (0.35 Hz to 7,500 Hz) neural signals were recorded at 25,000 samples/s/channel. The sessions lasted for 40–70 min, limited by the sedative effect of the initial injection. No additional drugs were administered during the sessions included in this study. The monkey was then returned to his cage and given an intramuscular injection of atipamezole (0.05 mg/kg) to reverse the effects of dexmedetomidine (Scheinin et al., 1998).

After each of the recording sessions in monkeys D and F (7 sessions), we set up a custom neurophysiology system, called the PennBMBI, prior to returning the animal to monitor neural activity during sedation reversal, wake, and sleep. The PennBMBI is a battery-powered device we developed previously for brain-machine interface applications (Liu et al., 2015). It recorded one wide-band (0.79 Hz to 2,500 Hz) neural signal at a rate of 10,000 samples/s. The data was saved to an onboard microSD card and retrieved the next time the monkey was brought to the lab. The device was housed in the same head-fixed chamber as the electrode connectors.

Separate sedated sessions were focused on quantifying neural connectivity. Bipolar electrical stimuli (biphasic, 0.3-ms/phase, charge-balanced pulses generated by an IZ2H stimulator, Tucker-Davis Technologies) were applied to adjacent pairs of PHG electrodes and the response on the HIPP array was recorded. In some sessions, we implemented a closed-loop recording and stimulating paradigm. The digital signal processors of the RZ2 were programmed to bandpass filter (e.g. 30–50 Hz) the recording from a chosen HIPP electrode, square the signal, and trigger a bipolar PHG stimulus pulse when the value exceeded a threshold. In this way we could study PHG-HIPP connectivity in consistent states defined by oscillatory activity.

To continue assessment of connectivity during sedation reversal and awake states, the PennBMBI was programmed to provide bipolar stimulation at fixed intervals (i.e. a stimulus

pulse every 30 s) and record the evoked response. The battery typically lasted for 3–4 h during stimulating-recording experiments and 18–30 h when just recording.

Not every experiment was conducted in each monkey. Monkey F was trained to sit in a chair and participate in awake behavioral studies. Thus sedated sessions were limited in him and no closed-loop electrophysiology tests were performed. Also, the wearable system was not available for monkey O. Thus all sleep, wake, and sedation reversal data were collected from monkeys D and F. For all monkeys, the experimental sessions included in this study were interleaved with sessions devoted to other objectives.

Data analysis

Neural signals were recorded in monopolar configuration referenced to shorted skull screws placed bilaterally over frontal and parietal cortex. To assess whether the field potentials were local to the HIPP and PHG or were a result of activity near the skull screws, we performed the analyses below both before and after re-referencing the signals. Specifically, the HIPP and PHG signals were re-referenced to an electrode on the depth arrays that was just posterior or anterior to these areas, typically localized to white matter. We found the results to be robust to the chosen reference, as the dominant slow and gamma rhythms were largely confined to the target areas.

Phase-amplitude coupling between different frequency bands was quantified with the modulation index (Tort et al., 2010). Briefly, the instantaneous amplitudes of one band and instantaneous phases of another were computed using the Hilbert transform. The mean amplitude in each of N = 16 phase bins was calculated and normalized by dividing by the sum across all bins. The result was an amplitude distribution, P, as a function of phase, θ. The modulation index, MI, was then defined as the Kullback-Leibler distance between that distribution and a uniform distribution:

$$MI = \frac{\log(N) + \sum_{j=1}^{N} P(j) \quad \log\left[P(j)\right]}{\log(N)}.$$

A disadvantage of using MI to quantify phase-amplitude coupling is that the index values, which were typically in the range of .001 to .05, do not give an intuitive sense of the absolute coupling strength. The values were small because the theoretical maximum, $MI = 1$, occurs in the unrealistic event that amplitudes are zero for all but one phase bin. We explored the use of a simpler and more intuitive metric of coupling: $MP = [\max(P)\text{-}\min(P)]/\max(P)*100$, which yields values ranging from 0 to 100% modulation. Our amplitude distributions occupied most of this range. However, unlike MI, MP is insensitivity to the width of the amplitude distribution (Tort et al., 2010). Furthermore, we found that variations in amplitude distribution width were present in our dataset. Specifically, P typically became narrower with increasing modulation. Thus, we chose to use the width-sensitive measure, MI. To provide a sense of absolute modulation, however, we calculated the relationship between MI and MP for the observed set of distributions. For reference, a MI of .001 = 18%, .005 = 36%, .01 = 48%, and .05 = 78%.

To exhaustively search for phase-amplitude coupling, *MI* was computed for a matrix of frequency band pairs to generate a comodulogram (Tort et al., 2010). In most cases, we searched 20 frequency bands for amplitude (logarithmically spaced between 10 Hz and 300 Hz) and 20 frequency bands for phase (logarithmically spaced between 0.1 Hz and 10 Hz).

To determine if each amplitude distribution was unimodal and had a preferred phase, θ_p, we fit P with a von Mises distribution, $\hat{P}(\theta) = a + b \exp[\kappa \cos(\theta - \theta_p)]$, using nonlinear least-squares to find the parameters a, b, κ, and θ_p. The goodness of fit was assessed by computing the coefficient of determination, R^2:

$$R^2 = 1 - \frac{\sum_{j=1}^{N} \left[P(j) - \hat{P}(j)\right]^2}{\sum_{j=1}^{N} \left[P(j) - \bar{P}\right]^2},$$

where $\bar{P}$ was the mean of P (Kvalseth, 1985). Preferred phase was reported only when $R^2 > 0.9$. Phases of 0 and 180 deg correspond to the peak and trough of the cycle, respectively.

We also computed gamma (30–50 Hz) amplitude distributions during different brain states (e.g. sedation versus awake). For 10-min blocks of time in each state, the instantaneous amplitude was computed with the Hilbert transform of the bandpass-filtered signal and compiled into empirical probability distributions. Power spectral densities were computed using Thomson's multitaper estimate using 5 Slepian tapers. Magnitude-squared coherence was computed using Welch's averaged modified periodogram method with 10-s windows and 50% overlap. The coherence significance was determined by a permutation test. The significance level was the 95th percentile of the distribution of coherence values (N = 1000) computed after randomly permuting samples in one of the signals.

To analyze sleep, no electrooculogram or electromyogram were available in these animals to score stages by traditional methods. However, as described in the Results, the inverse relationship between low-frequency (< 10 Hz) power and gamma (30–80 Hz) power during the night closely matched accounts of primate HIPP activity in identified sleep stages (Tamura et al., 2013; Takeuchi et al., 2015). Specifically, putative slow-wave sleep periods were identified by low gamma power and high low-frequency power.

The time-domain analysis of electrically-evoked potentials was performed without any digital filtering. The only data filters were imposed online by the acquisition hardware (0.2 Hz to 7.5 kHz passband). K-means clustering of the evoked potentials was performed on a window between 2 and 40 ms relative to the stimulus, which captured the waveform extent. The significance of oscillation phase on evoked potential amplitude was evaluated with a modification of the Rayleigh test for weighted vector data (Moore, 1980).

Results

Clinical depth electrode arrays were implanted chronically in the HIPP and PHG of three rhesus macaques (monkeys O, D, and F). In two of the monkeys, a third electrode array was implanted in deep medial structures including the septal nuclei and hypothalamus (Fig. 1A). Electrode placement was assessed through co-registered MR and CT images (Fig. 1B). Our

experiments began by assessing sleep-like oscillations induced by ketamine-dexmedetomidine sedation.

Gamma-slow oscillation coupling in sedation and sleep

Sedated recordings in the HIPP and PHG of all three monkeys had pronounced slow (0.5–2 Hz) and gamma (30–100 Hz) oscillations (Fig. 2A). These rhythms were reliably observed on all HIPP and PHG electrodes in sedated sessions spanning 3–8 weeks. Unlike some previous HIPP recordings in sedated primates and sleeping humans, theta (4–10 Hz) oscillations and sleep spindles were rarely observed in the recordings (Stewart and Fox, 1991; Staresina et al., 2015). Thus we focused our analysis on slow and gamma oscillations and their interaction.

The activity in HIPP and PHG was significantly coherent specifically at SO and gamma frequencies (Fig. 2B, left). Furthermore, both these rhythms were highly coherent along the longitudinal axis of the HIPP (Fig. 2B, right). Inspection of the raw data revealed that gamma oscillations occurred in bursts, usually just after the peak of SO cycles (Fig. 2C). To quantify this effect we computed the modulation index (*MI*), a measure of cross-frequency coupling that determines how the oscillation amplitude of one frequency band is modulated by oscillation phase of another band. The comodulograms showed modulation of gamma amplitude with SO phase in all three monkeys, although the effect was strongest in monkey D (Fig. 2D). A preferred phase analysis confirmed that gamma bursts occurred on the downslope of the SO cycles, with a mean preferred SO phase of 73.1 ± 11.4 deg (Fig. 2E). Strong gamma-SO coupling was observed in all electrodes localized to the HIPP or PHG. However, coupling was virtually absent in the medial areas accessed by the third electrode array in monkeys D and F (Fig. 2F).

Gamma-SO coupling was highest just after sedation and gradually decreased over the course of the recording sessions (Fig. 3A). Correspondingly, there was a gradual decrease in SO power (Fig. 3B). Conversely, there was generally a modest increase in gamma power over time (Fig. 3C). Consistent with a gating effect of SO cycles on gamma oscillations, the distribution of gamma amplitude during sedation appeared to be bimodal (Fig. 3D). The gamma power increase was a result of a relative change in the proportion of time spent in the two modes of the distribution.

Next, we assessed gamma-SO coupling during natural sleep. At the end of selected sedated sessions, a wearable battery-powered device was used to record from a chosen electrode during free behavior in the monkey's home cage. Spectrograms of the recorded activity showed typical wake-sleep patterns (Fig. 4 bottom). The overnight recordings during the 12-h period of darkness (19:00 to 07:00) had two main features. First, SO (0.5–2 Hz) and theta (4–10 Hz) power were strongly positively correlated ($r = 0.83$). Second, the low-frequency (<10 Hz) power was negatively correlated with gamma (30–80 Hz) power ($r = -0.70$). The low- and gamma-frequency power ratio defined two clear electrophysiological states that alternated throughout the night. These same cross-frequency power relationships were found by two prior studies of primate HIPP activity during sleep (Tamura et al., 2013; Takeuchi et al., 2015). Furthermore, these prior studies found that low- and gamma-frequency power corresponded to slow-wave sleep (SWS) and rapid eye movement (REM) sleep states,

respectively, as scored by traditional methods (Rechtschaffen and Kales, 1968). We thus adopted this interpretation. Without an electromyogram, we could not rule out the possibility that some of the putative REM states were in fact awake states (Tamura et al., 2013). Ultimately, however, those states were irrelevant to the investigation of gamma-SO coupling, which was restricted to SWS. The time-resolved *MI* revealed strong gamma-SO coupling specifically during SWS in HIPP recordings but not in septal nuclei recordings (Fig. 4 top). The comodulograms and preferred SO phase of the gamma oscillations during SWS and sedation were qualitatively similar (Fig. 4 insets). However, upon closer inspection, there were two main differences in phase-amplitude coupling between SWS and sedation. First, across 4 sessions in monkeys F and D in which a HIPP or PHG signal was recorded in both states, the gamma-SO *MI* was 6.5 to 11.8 times larger in sedation than SWS (Fig. 5A). Second, the gamma frequency whose amplitude was maximally coupled to the SO was significantly higher in SWS (72.1 ± 3.3 Hz) than sedation (40.9 ± 3.4 Hz; $t_6 = 13.5$, p = 1e-5; Fig. 5A). There was no significant difference in the SO frequency whose phase was maximally coupled to gamma amplitude (SWS = 0.97 ± 0.10 Hz; sedation = 0.95 ± 0.19 Hz; $t_6 = 0.23$, p = 0.823).

Several gamma sub-bands have been identified in the HIPP-PHG network, with distinct cellular mechanisms and functions (Colgin and Moser, 2010; Buzsaki and Wang, 2012). Multiple gamma generators could underlie the frequency difference in gamma-SO coupling between sedation and SWS. We asked whether the broad-frequency, SO-modulated gamma rhythm during sedation (e.g. Fig. 5A left) included a distinct high-gamma rhythm matching that seen in SWS. It was evident in the raw sedation data that a smaller-amplitude, higher-frequency oscillation often occurred near the peak of the SO cycle, prior to the 40-Hz oscillation occurring on the downslope of the cycle (Fig. 2C). Quantitatively, the amplitude distributions of low (30–50 Hz) and high (75–100 Hz) gamma activity as a function of SO phase showed a consistent phase shift (Fig. 5B). During sedation, the preferred SO phase of high-gamma activity was significantly closer to the peak of the SO cycle than that of low-gamma activity ($t_{18} = 9.2$, p = 3e-8; Fig. 5C). This phase distinction of gamma sub-bands is reminiscent of HIPP theta-gamma coupling in rodents (Belluscio et al., 2012). Finally, the preferred SO phase of high-gamma activity in sedation and sleep were statistically equivalent ($t_{22} = 0.2$, p = 0.84; Fig. 5C), which suggests that this rhythmic activity may be derived from the same mechanism in both states.

In summary, the results show that ketamine-dexmedetomidine sedation in macaques produces slow and gamma oscillations with phase-amplitude coupling in HIPP and PHG. Low- and high-gamma activity were coupled to distinct phases of the SO cycle. These features were similar to SWS, although only high-gamma coupling was present in sleep. The coupling was stronger in sedation than SWS, but the coupling strength gradually decreased as the sedative effects dissipated over time.

Sleep-like rhythms modulate PHG-HIPP connectivity

Co-modulated, gamma-slow rhythms during anesthesia and sleep in rodents are correlated with cyclically hyperpolarized and depolarized neuronal membrane potentials (Steriade et al., 1993b). We asked whether there was mesoscopic evidence of similar excitability changes

correlated with the sleep-like rhythms in sedated monkeys. To address this question, we examined effective PHG-HIPP connectivity and its modulation during sedation.

Connectivity between the PHG and HIPP was quantified with electrically-evoked potentials (EPs). Single, biphasic current pulses (0.3-ms/phase) were delivered between adjacent pairs of PHG electrodes and the response was recorded along the HIPP array. In each monkey, we identified at least one PHG electrode pair that produced a low-latency HIPP response. For example, in monkey D, stimuli evoked an EP with 6.98 ± 0.14 ms latency to peak (Fig. 6A). Based on their small latency variability and their ability to follow stimuli delivered at 50 Hz (data not shown), we interpreted these responses to be monosynaptic. However, the distribution of response waveforms to 100 stimuli, delivered at 0.2 Hz, was noticeably bimodal. K-means clustering of the evoked waveforms divided the responses into two groups: relatively large and biphasic EPs (N = 26) or small and monophasic EPs (N = 74) (Fig. 6A bottom).

The sequence of strong and weak monosynaptic responses might be explained by state-dependent excitability fluctuations in the PHG-HIPP network caused by the sleep-like rhythms. We hypothesized that the pattern of ongoing HIPP oscillations just prior to the stimulus time would predict the response. Indeed, gamma-dependence of the EPs could clearly be seen in the unprocessed voltage traces. Qualitatively, the EP was small (Fig. 6B top) or large (Fig. 6B bottom) depending on whether the stimulus occurred outside or inside a gamma burst, respectively. To quantify this effect, we computed the power spectrum in a 300-ms window preceding each stimulus. There were significant differences between the two response groups defined by the cluster analysis in pre-stimulus low (25–63 Hz) and high (76–210 Hz) gamma band power ($t_{98} > 2.6$, $p < .01$) (Fig. 6C). To further demonstrate the state-dependent strength of the PHG-hippocampal connection, we performed a closed-loop electrophysiology experiment. Gamma-band (30–50 Hz) power was estimated in real time and used to trigger PHG stimulation (see Methods). The resulting EPs had uniformly high amplitude (Fig. 6D).

These results from monkey D were replicated in monkey O. PHG stimuli evoked a small EP with 6.06 ± 0.15 ms latency to peak (Fig. 6E). Cluster analysis was used to divide trials into those with (N = 16) and without (N = 84) a biphasic EP (Fig. 6E bottom). The only significant differences in pre-stimulus power between trial clusters were again in the low (40–50 Hz) and high (68–98 Hz) gamma bands ($t_{98} > 2.6$, $p < .01$). Finally, triggering PHG stimuli from high-gamma (70–100 Hz) significantly increased the number (N = 28 vs. 16, $\chi_1 = 4.2$, $p = .04$) and amplitude (205 vs. 101 μV, $t_{42} = 7.1$, $p < .001$) of EPs in the high-amplitude cluster compared to the open-loop experiment (Fig. 6F).

To better quantify the relationship between pre-stimulus oscillatory activity and EP size, we performed an extended session in monkey D in which 500 stimulus pulses were delivered to the PHG over the course of 70 min. As in the prior sessions, the peak EP amplitude was distributed bimodally throughout the sedated session (Fig. 7A). The correlation between peak monosynaptic amplitudes and pre-stimulus power was computed in logarithmically spaced bands from 5 to 500 Hz (Fig. 7B). The results mirrored the inter-cluster power comparison shown in Figure 6C, with high correlations in the low and high gamma bands. A

maximum correlation of 0.67 was obtained with the 39–46 Hz band (Fig. 7C). The correlation coefficient for this gamma band, when computed for sequential 100-stimulus blocks, was consistent throughout the session with a range of 0.64 to 0.69.

The preceding analyses quantified pre-stimulus activity as the average power in the 300-ms window before the stimulus. However, the prior phase-amplitude coupling result predicts that EP amplitude should also be correlated with SO phase. Furthermore, previous studies have found that effective connectivity can be modulated by the specific SO (Schall et al., 2008) or gamma (Ni et al., 2016) phase at the time of the stimulus. Thus, we computed the phase and amplitude of the gamma or SO cycle occurring immediately before each stimulus (Fig. 7D). The oscillatory cycles prior to the stimuli were within the gamma and SO frequency range on 210/500 and 263/500 occasions, respectively. The EP peak was not significantly modulated by gamma phase (Rayleigh test, $p = .665$, Fig. 7E). As in the average power analysis, the EP peak was linearly correlated with the log-transformed gamma cycle amplitude ($r = .63$, Fig. 7F). As predicted by the presence of phase-amplitude coupling, the EP peak was unimodally tuned to SO phase (Rayleigh test, $p = .002$, Fig. 7G). The monosynaptic responses were on average largest at a phase of 51.6 deg on the downward slope of the SO cycle (Fig. 7G top), similar to the preferred phase of gamma coupling. Finally, the EP peak was not correlated with SO amplitude ($r = .08$, Fig. 7H).

Taken together, these results demonstrate that sleep-like, gamma-SO coupling during sedation was correlated with excitability changes in the PHG-HIPP network. Specifically, gamma bursts after the peak of SO cycles corresponded to periods of increased gain of monosynaptic connections between these areas.

PHG-HIPP connectivity during sedation reversal and wake

Sedation produced two discrete PHG-HIPP connectivity gains correlated with the coupled gamma-SO cycles. Our final analysis addressed how these gains evolved during sedation reversal and how they compared to the awake state. The open-loop stimulation protocol from Figure 6A was repeated approximately two months later in monkey D under sedation. Again, a bimodal distribution of monosynaptic response amplitudes was seen (Fig. 8A top, red and black circles). Pre-stimulus gamma band power was significantly higher ($t_{98} = 4.1$, $p = .0001$) for the higher response amplitude group (Fig. 8A bottom, red and black circles). These results demonstrate the reproducibility and stability of the effects. At the end of the sedated session, the wearable electrophysiology device was configured to continue collecting EP data as the animal woke up and began behaving freely in his home cage. The device delivered a single stimulus pulse (0.5 mA, 0.3 ms/phase; same as during sedation) every 30 s and saved the HIPP response. Once the device was configured and running, monkey D was returned to his home cage and given atipamezole to reverse the effects of dexmedetomidine. The recovery period was characterized by a transient increase in HIPP gamma-band activity and steady increase in peak amplitude of the EP (Fig. 8A, gray circles). Note the uncorrelated nature of these variables during recovery, unlike during sedation. Subsequently, when the animal was fully recovered, the peak amplitude plateaued at a higher level than seen during sedation and was distributed unimodally, not bimodally (Fig. 8A, blue circles). Pre-stimulus low-gamma power, on the other hand, returned to a

level not significantly different from that which led to larger responses during sedation (t_{222} = 0.6, p = .56) but higher than the pre-stimulus power of the smaller sedated response group (t_{230} = 1.9, p = .05).

Thus, the gamma-dependence of evoked HIPP responses was specific to the sedated state and the responses overall were weaker than during the awake state (Fig. 8B). These results were replicated in monkey F, who was trained to be brought to the lab awake. During an awake session, PHG stimuli evoked a consistently large monosynaptic hippocampal response with population spike (Fig. 8C, blue). On a subsequent sedated session, the same stimuli evoked much smaller, bimodally distributed responses with significantly higher 30–42 Hz power (t_{48} > 2.0, p < .05) prior to the larger response (Fig. 8C, black and red). Monkey F also exhibited similar HIPP oscillatory activity during recovery from sedation as monkey D, with a transient (~15 min) increase in gamma power and decrease in low-frequency (<10 Hz) power relative to the awake state (Fig. 8D). Lastly, the results of Figure 8A indicate that the state-dependent connectivity effect of sedation was primarily due to periods of decreased gamma activity relative to awake, likely due to the inhibitory phases of the SO cycle characterized previously. This result was based on gamma power calculated in the 300-ms window prior to stimulus pulses in the sedated and awake states. A similar result was obtained by compiling the distribution of gamma amplitudes at all time points across 1-h sedated versus awake recordings in monkey F (Fig. 8E). The higher mode of the sedation distribution (red) aligned with the awake gamma amplitude distribution (blue), while the lower mode (black) was not present in the awake distribution.

In summary, the two PHG-HIPP connectivity gains during sedation were both substantially lower than that of the awake state. During sedation recovery, there was a gradual increase in gain and an uncorrelated, phasic increase in gamma power. Pre-stimulus gamma power was predictive of the relative gain difference during sedation but not the absolute difference from wake.

Discussion

The main finding of this study is that ketamine-dexmedetomidine sedation in primates produces phase-amplitude coupling of gamma and slow oscillations in the PHG-HIPP network. The effect was similar to but stronger than coupling seen in natural SWS. The SO cycles produced periods of regular and abnormally low gamma activity relative to awake activity, which were correlated with two discrete HIPP response gains to PHG input. Reversal of sedation caused decreased SO power, abnormally increased gamma power, and a gradual strengthening of PHG-HIPP connectivity.

Slow oscillations and neuronal excitability

The connectivity results are consistent with documented effects of neocortical SO on the PHG and HIPP during anesthesia in cats and rodents. The SO is an intrinsic rhythm of the neocortex (Steriade et al., 1993a; Timofeev et al., 2000). The rhythm is synchronous across most of the cortex, due to long-range recurrent cortical and possibly thalamic connections (Amzica and Steriade, 1995). In a large percentage of neocortical neurons, each SO cycle corresponds to an UP state of depolarized membrane potential with spiking activity and

gamma oscillations followed by a DOWN state of hyperpolarized membrane potential and an absence of spiking activity and gamma oscillations (Steriade et al., 1993b; Steriade, 2006).

UP-DOWN states synchronous with neocortical SO are also present in pyramidal neurons in both superficial and deep layers of the entorhinal cortex (EC) in anesthetized rodents (Isomura et al., 2006; Hahn et al., 2012). It is likely that through entorhinal and other PHG inputs the neocortical SO affects the HIPP (Wolansky et al., 2006). The effect, however, is somewhat different than in cortical neurons. Neurons in the dentate gyrus (DG), CA3, and CA1 show little or no UP-DOWN membrane potential fluctuations during neocortical SO (Isomura et al., 2006; Hahn et al., 2007). Cortical DOWN-UP transitions are associated with monosynaptic excitatory input from PHG to the DG and CA1. Correspondingly, most DG and CA1 neurons have more spiking activity in the UP state. Furthermore, similar to our results (Fig. 7G), the evoked DG response to perforant path stimulation is maximal during the falling phase of SO cycles (Schall et al., 2008). In contrast, most CA3 and some CA1 neurons preferentially discharge in the DOWN state. Gamma oscillations also occur in the UP state in DG and in the CA1 stratum lacunosum-moleculare, which receives direct cortical inputs. However, gamma oscillations are most prominent in the DOWN state in the CA1 stratum radiatum, which receives inputs from CA3 (Isomura et al., 2006).

To summarize, the anesthetized rodent literature shows that the neocortical SO produces synchronous rhythmic excitation and inhibition of PHG neurons and their monosynaptic HIPP targets. This would explain the two HIPP response gains to monosynaptic PHG input observed in our study and their correlation with gamma amplitude and SO phase. Interestingly, the low-amplitude response state in monkey D consistently had a late component of the EP around 20 ms not seen in the high-amplitude response state (e.g. Fig. 8B, black vs. red response). This late component may be a disynaptic response along the PHG-CA3-CA1 pathway (Yeckel and Berger, 1990), which was not observed in either state in the other animals perhaps due to electrode placement differences. An increased disynaptic response during the low-gamma, inhibitory phase of SO cycles is consistent with DOWN-state excitation of CA3 (Isomura et al., 2006). Characterizing trisynaptic pathway excitability during the SO in primates is an avenue for future investigation. Overall, our study shows that there is a strong similarity between rodents and primates in the effects of the SO on PHG and HIPP excitability.

Mechanisms of gamma-SO coupling

From our results, we can also infer a potential mechanism for gamma-SO coupling. First, we can rule out a mechanism where gamma power simply reflects asynchronous spiking activity that, as described above, is elevated in UP states. The spectral power, coherence, and comodulograms demonstrate that the coupled gamma power was a band-limited oscillation rather than the broadband power increase one would expect if due to spiking activity (Ray and Maunsell, 2011). The specificity of the coupling to PHG and HIPP suggests that the SO modulates gamma generators intrinsic to this network. Extensive work in rodents has identified two such gamma generators: a fast gamma (~80 Hz) generator in the PHG and a slow gamma (~40 Hz) generator in CA3 (Colgin and Moser, 2010). These rhythms are

thought to arise largely from inhibitory interneuron activity producing gamma-frequency inhibitory postsynaptic potentials in pyramidal cells (Buzsaki and Wang, 2012). SO modulation of these generators could be due to increased/decreased excitatory drive to inhibitory networks during UP/DOWN states. The slow gamma rhythm of the CA3 generator is predominant in anesthetized rodents and slice preparations in which PHG-HIPP connectivity is reduced (Colgin and Moser, 2010). Likewise, here we found that ketamine-dexmedetomidine sedation produced a net decrease in PHG-HIPP connectivity and a SO-modulated gamma rhythm that was slower (40.9 Hz) than in natural SWS (72.1 Hz). Thus our results point to a similar arrangement of distinct PHG and HIPP gamma generators in the primate, both of which are influenced by the SO.

HIPP gamma-SO coupling may also be related to memory consolidation via sharp-wave-ripple (SWR) complexes. SWRs are intrinsic HIPP events during which prior, behaviorally-related sequences of HIPP spiking activity are reactivated (Kudrimoti et al., 1999; Csicsvari et al., 2000). SWRs are biased to occur during neocortical UP states (Battaglia et al., 2004; Molle et al., 2006), which may facilitate both remote replay of HIPP spiking sequences in the neocortex and, ultimately, memory consolidation (Ji and Wilson, 2007). In primates and humans, the ripple oscillation has a lower frequency range (~80–130 Hz) than in rodents (Bragin et al., 1999; Clemens et al., 2007; Skaggs et al., 2007; Leonard et al., 2015; Ramirez-Villegas et al., 2015). This mechanism could, therefore, explain the fast gamma-SO coupling we observed in SWS. However, we have no definitive data suggesting the SO-modulated gamma were, in fact, ripples. Furthermore, given that ripples are not coherent across HIPP subfields (Sullivan et al., 2011), we would have been less likely to record them due to the extensive spatial averaging from our macroelectrodes. Recent studies have found that a transient slow gamma oscillation occurs during SWR events and that, unlike ripples, it is synchronous within the HIPP and between the HIPP and neocortex (Carr et al., 2012; Remondes and Wilson, 2015; Greenberg et al., 2016). To the extent SWR are biased by the SO, this slow gamma rhythm could also underlie the observed coupling and, by virtue of its synchrony, be theoretically more visible in our recordings.

A primate model of sleep-like HIPP activity

Two recent studies were the first to examine macaque HIPP activity during natural sleep with detailed sleep stage classification (Tamura et al., 2013; Takeuchi et al., 2015). High-amplitude slow, delta, and theta (0.5–8 Hz) oscillations were found to be present predominantly in stages III and IV of non-rapid eye movement sleep (Tamura et al., 2013). The corresponding epochs in our sleep recordings were precisely those with strong gamma-SO coupling. Our sleep phase-amplitude coupling results mirror those of Takeuchi et al. They found gamma-SO coupling largely confined to stages III and IV, with a similar preferred phase and gamma frequency range as we observed (Takeuchi et al., 2015).

Ours is the first study to directly compare macaque HIPP field potentials in sleep to sedation. It has long been observed that ketamine, usually in combination with an α_2-adrenergic receptor agonist (e.g. xylazine, dexmedetomidine), can produce SWS-like activity in the HIPP of non-primates (Sharma et al., 2010). There is evidence that the ketamine-induced SO in the HIPP is a result of NMDA-receptor antagonism in the nucleus

reuniens (Zhang et al., 2012). The SO is also a common electroencephalography (EEG) feature of dexmedetomidine sedation in humans (Purdon et al., 2015; Akeju et al., 2016). Thus both agents may have contributed to generation of the observed SO. Ketamine, given alone, is also typically associated with increased gamma activity in the HIPP (Lazarewicz et al., 2010; Kittelberger et al., 2012). We observed no gamma amplitude increase relative to wake (e.g. Fig. 8E), perhaps due to a counterbalancing suppression of gamma oscillations by dexmedetomidine. Such an action can be inferred from the prominent increase in gamma power immediately after administration of the reversal agent atipamezole (Jang et al., 2009).

As in a prior investigation in cats (Chauvette et al., 2011), we found that there were several differences between neural activity in sedation and sleep that must be considered if using ketamine-dexmedetomidine to model SWS in primates. First, a slower gamma oscillation was coupled to the SO during sedation as compared to SWS. As discussed above, this could result from sedation decreasing the normal contribution of the PHG to gamma generation in the HIPP. Second, the strength of phase-amplitude coupling in sedation was artificially elevated relative to SWS. This result is similar to that of a prior study, which found that ketamine increased theta-gamma coupling in rat HIPP (Caixeta et al., 2013). The result is also reminiscent of the EEG “extreme delta brush” pattern, a high-amplitude 20–30 Hz burst occurring on the descending phase of 1–3 Hz waves, seen in some human cases of anti-NMDA receptor encephalitis (Schmitt et al., 2012). We speculate that there may be a general link between NMDA-receptor hypofunction and the hyper-modulation of local fast (beta/gamma) oscillations by slow rhythms. Finally, a practical challenge in this SWS model is the stability of the effects. SO power and gamma-SO coupling was a moving target, steadily decreasing after sedation as in other anesthetized preparations (Wolansky et al., 2006).

In light of these considerations, the ketamine-dexmedetomidine primate model could be viewed as an opportunity to study the electrophysiology of the putative, intrinsic CA3-CA1 gamma and SWR generators in relative isolation from PHG inputs. Analogous investigations in anesthetized rodents have provided tremendous information about intrinsic HIPP physiology. Primate HIPP function in natural SWS, on the other hand, would best be studied directly through further enhancements (e.g. channel count, sampling rate, power efficiency) to wearable electrophysiology devices like those used here.

Acknowledgements

Support was provided in part by the DARPA Restoring Active Memory (RAM) program (Cooperative Agreement N66001-14-2-4032). The views, opinions, and findings expressed are those of the authors and should not be interpreted as representing the official views or policies of the Department of Defense or the U.S. Government. We thank Michael Kahana and Daniel Rizzuto for initial guidance on this project.

References

Akeju O, Kim SE, Vazquez R, Rhee J, Pavone KJ, Hobbs LE, Purdon PL, Brown EN. 2016 Spatiotemporal Dynamics of Dexmedetomidine-Induced Electroencephalogram Oscillations. PLoS One 11(10):e0163431. [PubMed: 27711165]

Amzica F, Steriade M. 1995 Disconnection of intracortical synaptic linkages disrupts synchronization of a slow oscillation. J Neurosci 15(6):4658–77. [PubMed: 7790931]

Avants BB, Epstein CL, Grossman M, Gee JC. 2008 Symmetric diffeomorphic image registration with cross-correlation: evaluating automated labeling of elderly and neurodegenerative brain. Med Image Anal 12(1):26–41. [PubMed: 17659998]

Battaglia FP, Sutherland GR, McNaughton BL. 2004 Hippocampal sharp wave bursts coincide with neocortical “up-state” transitions. Learn Mem 11(6):697–704. [PubMed: 15576887]

Bekelis K, Desai A, Kotlyar A, Thadani V, Jobst BC, Bujarski K, Darcey TM, Roberts DW. 2013 Occipitotemporal hippocampal depth electrodes in intracranial epilepsy monitoring: safety and utility. J Neurosurg 118(2):345–52. [PubMed: 23082879]

Belluscio MA, Mizuseki K, Schmidt R, Kempter R, Buzsaki G. 2012 Cross-frequency phase-phase coupling between theta and gamma oscillations in the hippocampus. J Neurosci 32(2):423–35. [PubMed: 22238079]

Bragin A, Engel J Jr., Wilson CL, Fried I, Buzsaki G 1999 High-frequency oscillations in human brain. Hippocampus 9(2):137–42. [PubMed: 10226774]

Buzsaki G, Wang XJ. 2012 Mechanisms of gamma oscillations. Annu Rev Neurosci 35:203–25. [PubMed: 22443509]

Caixeta FV, Cornelio AM, Scheffer-Teixeira R, Ribeiro S, Tort AB. 2013 Ketamine alters oscillatory coupling in the hippocampus. Sci Rep 3:2348. [PubMed: 23907109]

Carr MF, Karlsson MP, Frank LM. 2012 Transient slow gamma synchrony underlies hippocampal memory replay. Neuron 75(4):700–13. [PubMed: 22920260]

Chauvette S, Crochet S, Volgushev M, Timofeev I. 2011 Properties of slow oscillation during slow-wave sleep and anesthesia in cats. J Neurosci 31(42):14998–5008. [PubMed: 22016533]

Clemens Z, Molle M, Eross L, Barsi P, Halasz P, Born J. 2007 Temporal coupling of parahippocampal ripples, sleep spindles and slow oscillations in humans. Brain 130(Pt 11):2868–78. [PubMed: 17615093]

Colgin LL, Moser EI. 2010 Gamma oscillations in the hippocampus. Physiology (Bethesda) 25(5): 319–29. [PubMed: 20940437]

Csicsvari J, Hirase H, Mamiya A, Buzsaki G. 2000 Ensemble patterns of hippocampal CA3-CA1 neurons during sharp wave-associated population events. Neuron 28(2):585–94. [PubMed: 11144366]

Destexhe A, Sejnowski TJ. 2003 Interactions between membrane conductances underlying thalamocortical slow-wave oscillations. Physiol Rev 83(4):1401–53. [PubMed: 14506309]

Diekelmann S, Born J. 2010 The memory function of sleep. Nat Rev Neurosci 11(2):114–26. [PubMed: 20046194]

Greenberg A, Whitten TA, Dickson CT. 2016 Stimulating forebrain communications: Slow sinusoidal electric fields over frontal cortices dynamically modulate hippocampal activity and cortico-hippocampal interplay during slow-wave states. Neuroimage 133:189–206. [PubMed: 26947518]

Hahn TT, McFarland JM, Berberich S, Sakmann B, Mehta MR. 2012 Spontaneous persistent activity in entorhinal cortex modulates cortico-hippocampal interaction in vivo. Nat Neurosci 15(11): 1531–8. [PubMed: 23042081]

Hahn TT, Sakmann B, Mehta MR. 2007 Differential responses of hippocampal subfields to cortical up-down states. Proc Natl Acad Sci U S A 104(12):5169–74. [PubMed: 17360347]

Huber R, Ghilardi MF, Massimini M, Tononi G. 2004 Local sleep and learning. Nature 430(6995):78–81. [PubMed: 15184907]

Isomura Y, Sirota A, Ozen S, Montgomery S, Mizuseki K, Henze DA, Buzsaki G. 2006 Integration and segregation of activity in entorhinal-hippocampal subregions by neocortical slow oscillations. Neuron 52(5):871–82. [PubMed: 17145507]

Jang HS, Choi HS, Lee SH, Jang KH, Lee MG. 2009 Evaluation of the anaesthetic effects of medetomidine and ketamine in rats and their reversal with atipamezole. Vet Anaesth Analg 36(4): 319–27. [PubMed: 19470142]

Jenkinson M, Bannister P, Brady M, Smith S. 2002 Improved optimization for the robust and accurate linear registration and motion correction of brain images. Neuroimage 17(2):825–41. [PubMed: 12377157]

Ji D, Wilson MA. 2007 Coordinated memory replay in the visual cortex and hippocampus during sleep. Nat Neurosci 10(1):100–7. [PubMed: 17173043]

Kittelberger K, Hur EE, Sazegar S, Keshavan V, Kocsis B. 2012 Comparison of the effects of acute and chronic administration of ketamine on hippocampal oscillations: relevance for the NMDA receptor hypofunction model of schizophrenia. Brain Struct Funct 217(2):395–409. [PubMed: 21979451]

Kudrimoti HS, Barnes CA, McNaughton BL. 1999 Reactivation of hippocampal cell assemblies: effects of behavioral state, experience, and EEG dynamics. J Neurosci 19(10):4090–101. [PubMed: 10234037]

Kvalseth TO. 1985 Cautionary Note About R2. American Statistician 39(4):279–285.

Lazarewicz MT, Ehrlichman RS, Maxwell CR, Gandal MJ, Finkel LH, Siegel SJ. 2010 Ketamine modulates theta and gamma oscillations. J Cogn Neurosci 22(7):1452–64. [PubMed: 19583475]

Leonard TK, Mikkila JM, Eskandar EN, Gerrard JL, Kaping D, Patel SR, Womelsdorf T, Hoffman KL. 2015 Sharp Wave Ripples during Visual Exploration in the Primate Hippocampus. J Neurosci 35(44):14771–82. [PubMed: 26538648]

Liu X, Zhang M, Subei B, Richardson AG, Lucas TH, Van der Spiegel J. 2015 The PennBMBI: Design of a General Purpose Wireless Brain-Machine-Brain Interface System. IEEE Trans Biomed Circuits Syst 9(2):248–58. [PubMed: 25769171]

Marshall L, Helgadottir H, Molle M, Born J. 2006 Boosting slow oscillations during sleep potentiates memory. Nature 444(7119):610–3. [PubMed: 17086200]

Molle M, Yeshenko O, Marshall L, Sara SJ, Born J. 2006 Hippocampal sharp wave-ripples linked to slow oscillations in rat slow-wave sleep. J Neurophysiol 96(1):62–70. [PubMed: 16611848]

Moore BR. 1980 A Modification of the Rayleigh Test for Vector Data. Biometrika 67(1):175–180.

Ni J, Wunderle T, Lewis CM, Desimone R, Diester I, Fries P. 2016 Gamma-Rhythmic Gain Modulation. Neuron 92(1):240–251. [PubMed: 27667008]

Purdon PL, Sampson A, Pavone KJ, Brown EN. 2015 Clinical Electroencephalography for Anesthesiologists: Part I: Background and Basic Signatures. Anesthesiology 123(4):937–60. [PubMed: 26275092]

Ramirez-Villegas JF, Logothetis NK, Besserve M. 2015 Diversity of sharp-wave-ripple LFP signatures reveals differentiated brain-wide dynamical events. Proc Natl Acad Sci U S A 112(46):E6379–87. [PubMed: 26540729]

Ray S, Maunsell JH. 2011 Different origins of gamma rhythm and high-gamma activity in macaque visual cortex. PLoS Biol 9(4):e1000610. [PubMed: 21532743]

Rechtschaffen A, Kales A. 1968 A manual of standardized terminology, techniques, and scoring system for sleep stages of human subjects. Washington, D.C.: Public Health Service, U. S. Government Printing Office

Remondes M, Wilson MA. 2015 Slow-gamma Rhythms Coordinate Cingulate Cortical Responses to Hippocampal Sharp-Wave Ripples during Wakefulness. Cell Rep 13(7):1327–35. [PubMed: 26549454]

Rohlfing T, Kroenke CD, Sullivan EV, Dubach MF, Bowden DM, Grant KA, Pfefferbaum A. 2012 The INIA19 Template and NeuroMaps Atlas for Primate Brain Image Parcellation and Spatial Normalization. Front Neuroinform 6:27. [PubMed: 23230398]

Schall KP, Kerber J, Dickson CT. 2008 Rhythmic constraints on hippocampal processing: state and phase-related fluctuations of synaptic excitability during theta and the slow oscillation. J Neurophysiol 99(2):888–99. [PubMed: 18046004]

Scheinin H, Aantaa R, Anttila M, Hakola P, Helminen A, Karhuvaara S. 1998 Reversal of the sedative and sympatholytic effects of dexmedetomidine with a specific alpha2-adrenoceptor antagonist atipamezole: a pharmacodynamic and kinetic study in healthy volunteers. Anesthesiology 89(3): 574–84. [PubMed: 9743392]

Schmitt SE, Pargeon K, Frechette ES, Hirsch LJ, Dalmau J, Friedman D. 2012 Extreme delta brush: a unique EEG pattern in adults with anti-NMDA receptor encephalitis. Neurology 79(11):1094–100. [PubMed: 22933737]

Sharma AV, Wolansky T, Dickson CT. 2010 A comparison of sleeplike slow oscillations in the hippocampus under ketamine and urethane anesthesia. J Neurophysiol 104(2):932–9. [PubMed: 20538775]

Siapas AG, Wilson MA. 1998 Coordinated interactions between hippocampal ripples and cortical spindles during slow-wave sleep. Neuron 21(5):1123–8. [PubMed: 9856467]

Skaggs WE, McNaughton BL, Permenter M, Archibeque M, Vogt J, Amaral DG, Barnes CA. 2007 EEG sharp waves and sparse ensemble unit activity in the macaque hippocampus. J Neurophysiol 98(2):898–910. [PubMed: 17522177]

Staresina BP, Bergmann TO, Bonnefond M, van der Meij R, Jensen O, Deuker L, Elger CE, Axmacher N, Fell J. 2015 Hierarchical nesting of slow oscillations, spindles and ripples in the human hippocampus during sleep. Nat Neurosci 18(11):1679–86. [PubMed: 26389842]

Steriade M 2006 Grouping of brain rhythms in corticothalamic systems. Neuroscience 137(4):1087–106. [PubMed: 16343791]

Steriade M, Nunez A, Amzica F. 1993a Intracellular analysis of relations between the slow (< 1 Hz) neocortical oscillation and other sleep rhythms of the electroencephalogram. J Neurosci 13(8): 3266–83. [PubMed: 8340807]

Steriade M, Nunez A, Amzica F. 1993b A novel slow (< 1 Hz) oscillation of neocortical neurons in vivo: depolarizing and hyperpolarizing components. J Neurosci 13(8):3252–65. [PubMed: 8340806]

Stewart M, Fox SE. 1991 Hippocampal theta activity in monkeys. Brain Res 538(1):59–63. [PubMed: 2018932]

Sullivan D, Csicsvari J, Mizuseki K, Montgomery S, Diba K, Buzsaki G. 2011 Relationships between hippocampal sharp waves, ripples, and fast gamma oscillation: influence of dentate and entorhinal cortical activity. J Neurosci 31(23):8605–16. [PubMed: 21653864]

Suthana N, Fried I. 2014 Deep brain stimulation for enhancement of learning and memory. Neuroimage 85 Pt 3:996–1002. [PubMed: 23921099]

Takeuchi S, Mima T, Murai R, Shimazu H, Isomura Y, Tsujimoto T. 2015 Gamma Oscillations and Their Cross-frequency Coupling in the Primate Hippocampus during Sleep. Sleep 38(7):1085–91. [PubMed: 25669188]

Tamura R, Nishida H, Eifuku S, Fushiki H, Watanabe Y, Uchiyama K. 2013 Sleep-stage correlates of hippocampal electroencephalogram in primates. PLoS One 8(12):e82994. [PubMed: 24386134]

Timofeev I, Grenier F, Bazhenov M, Sejnowski TJ, Steriade M. 2000 Origin of slow cortical oscillations in deafferented cortical slabs. Cereb Cortex 10(12):1185–99. [PubMed: 11073868]

Tort AB, Komorowski R, Eichenbaum H, Kopell N. 2010 Measuring phase-amplitude coupling between neuronal oscillations of different frequencies. J Neurophysiol 104(2):1195–210. [PubMed: 20463205]

Wolansky T, Clement EA, Peters SR, Palczak MA, Dickson CT. 2006 Hippocampal slow oscillation: a novel EEG state and its coordination with ongoing neocortical activity. J Neurosci 26(23):6213–29. [PubMed: 16763029]

Wu C, LaRiviere MJ, Laxpati N, Evans JJ, Gross RE, Sharan AD. 2014 Extraventricular long-axis cannulation of the hippocampus: technical considerations. Neurosurgery 10 Suppl 2:325–32; discussion 332–3.

Yeckel MF, Berger TW. 1990 Feedforward excitation of the hippocampus by afferents from the entorhinal cortex: redefinition of the role of the trisynaptic pathway. Proc Natl Acad Sci U S A 87(15):5832–6. [PubMed: 2377621]

Zhang Y, Yoshida T, Katz DB, Lisman JE. 2012 NMDAR antagonist action in thalamus imposes delta oscillations on the hippocampus. J Neurophysiol 107(11):3181–9. [PubMed: 22423006]

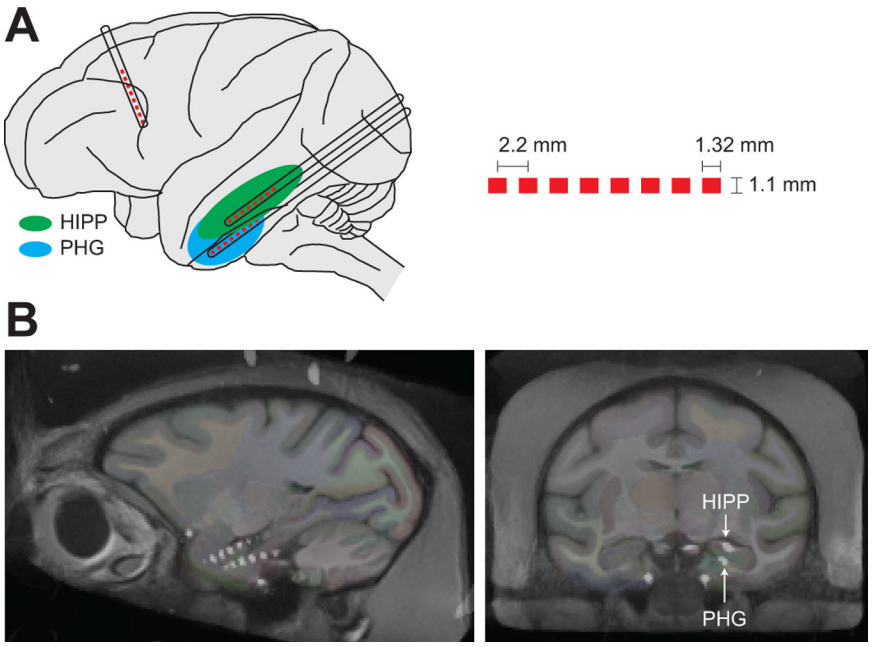

Figure 1.

Electrode implant. **A**, Illustration of the implanted depth electrode arrays. Pt electrodes are shown as red boxes and the electrode trajectories are shown as black outlined rectangles. The dimensions of the electrode arrays are shown on the right. **B**, Representative sagittal and coronal CT images from monkey F overlaid on the NeuroMaps brain atlas, showing the location of the implanted arrays targeting the HIPP and PHG.

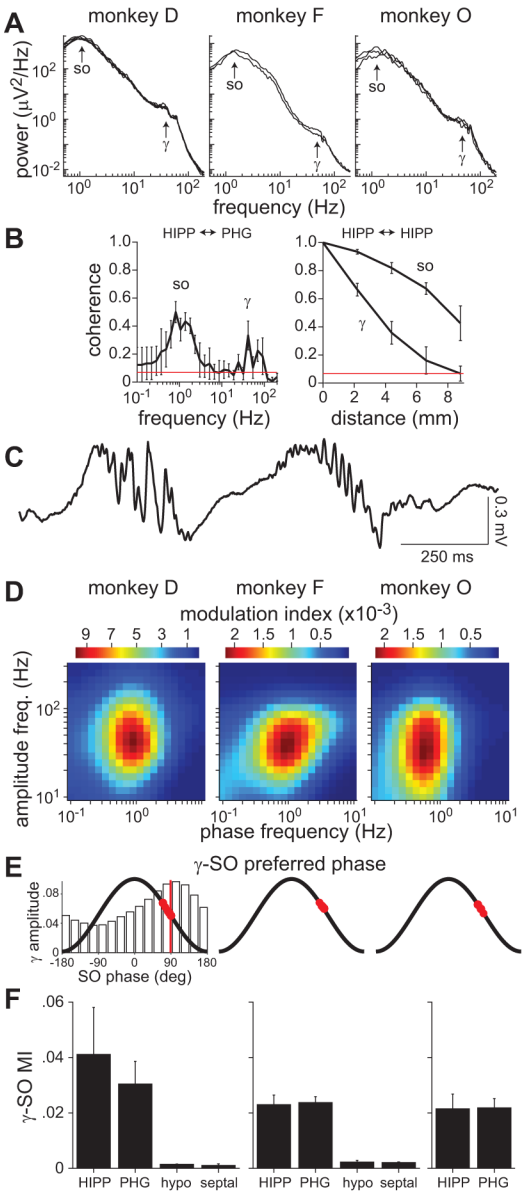

Figure 2.

Gamma-SO coupling during sedation. **A**, Power spectra of recordings from a HIPP electrode approximately 10–20 min after sedation. Spectra for multiple sedation sessions are shown (monkey D = 5 sessions, F = 2, O = 3). The same spectral features were seen on all other electrodes localized to the HIPP and PHG. **B**, Magnitude-squared coherence between HIPP and PHG activity (left) and between HIPP sites along the longitudinal axis (right). The mean coherence (± standard deviation, SD) across sessions is shown. Red line indicates coherence significance at the 95% level. **C**, Example segment of a HIPP recording from monkey D showing gamma bursts on the downslope of SO cycles. **D**, Comodulograms of HIPP activity in one sedated session for each monkey. The results were similar for all sessions. The color map indicates the modulation index, a measure of phase-amplitude coupling. **E**, Preferred SO (0.5–2 Hz) phase of gamma (30–80 Hz) oscillations. Red circles indicate the preferred

phase for each HIPP and PHG electrode. The bar graph on the left is an example normalized gamma amplitude distribution from which preferred phases were computed. The vertical red line indicates the preferred phase for this distribution, which corresponds to the pixel with highest MI in the left comodulogram in D. **F**, Mean modulation index (± SD) between gamma amplitude and SO phase across electrodes grouped by anatomical location (HIPP, PHG, hypothalamus, septal nuclei). Note that monkey O (right) only had electrodes in the HIPP and PHG.

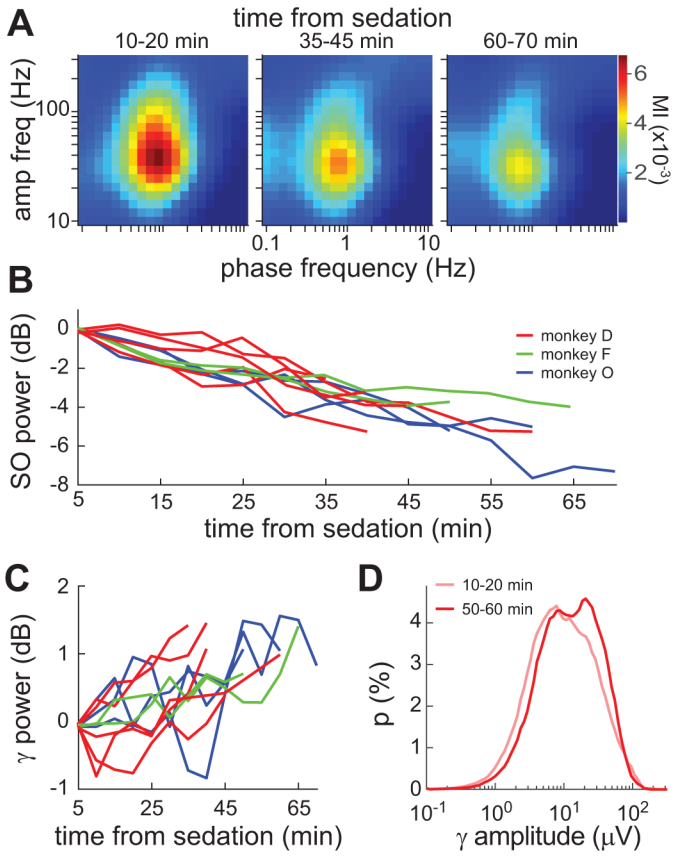

Figure 3.

Time-dependent oscillatory changes during sedation. **A**, Comodulograms of HIPP activity at the beginning, middle, and end of a 70-min sedated session. Results were similar in other sessions. **B**, Mean 0.5–2 Hz power computed in sequential 5-min windows over the duration of 10 sedated sessions. **C**, Same as B, but for 30–50 Hz power. **D**, Distribution of gamma (30–50 Hz) amplitude at the beginning and end of a sedated session with monkey D.

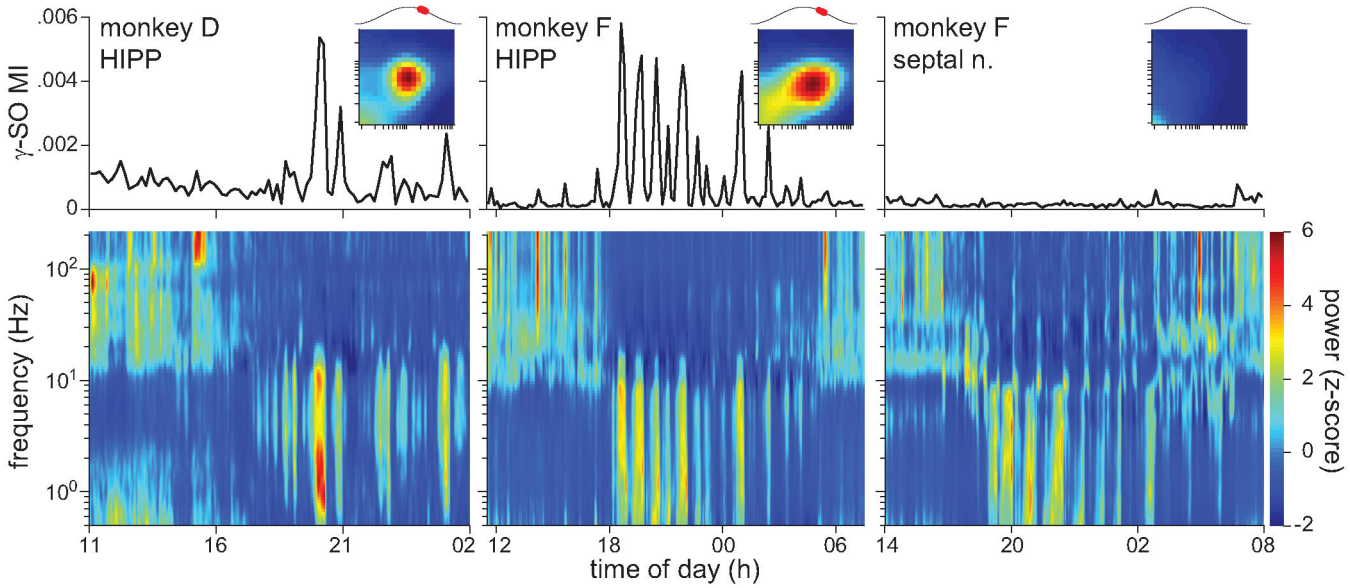

Figure 4.

Gamma-SO coupling during sleep. The spectrogram (bottom) and corresponding time-resolved gamma-SO modulation index (top) are shown for 3 separate recording sessions as monkeys were freely behaving in their home cage. The sessions differed by monkey or recording area, as indicated. Power in each frequency band was z-scored. The MI was computed in sequential 10-min windows. Insets show comodulograms and preferred SO phase of gamma activity for the SWS epochs. The x and y axes of the comodulograms are the same as in Fig. 2D and dark red corresponds to an MI of .0012 in monkey D and .0006 in monkey F.

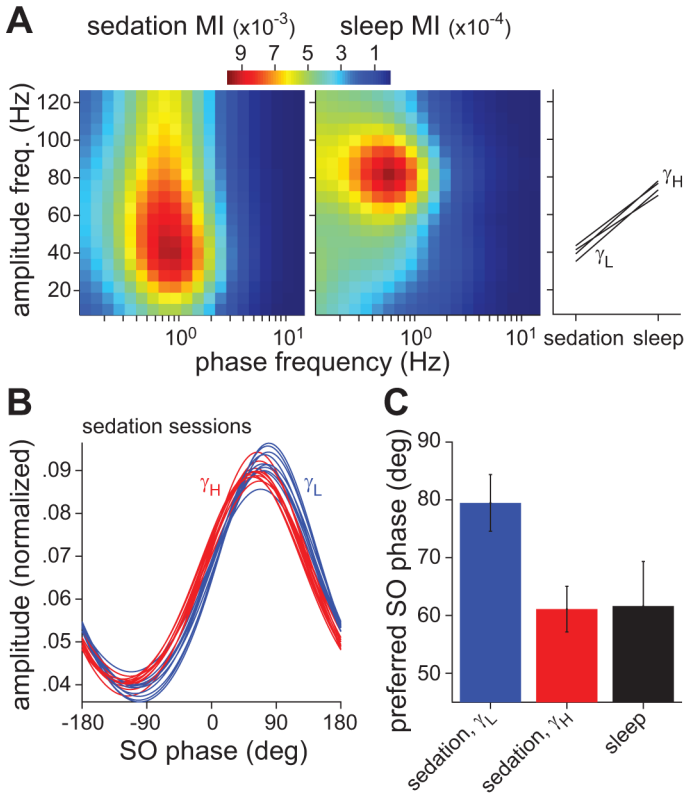

Figure 5.

Multiple gamma rhythms coupled to the SO during sedation and sleep. **A**, Comodulograms of activity recorded on the same HIPP electrode during sedation (left) and SWS (middle) in monkey D. Gamma-SO coupling was 10 times stronger during sedation. In addition, the gamma rhythm with peak coupling to SO phase had a frequency of 30–50 Hz (γ_L) in sedation and 75–100 Hz (γ_H) in sleep. This gamma frequency difference was consistent across the 4 sessions in monkeys D and F in which a HIPP or PHG signal was recorded in both states (right). **B**, Low (blue) and high (red) gamma amplitude as a function of SO phase for all sedated sessions. Mean amplitude in each SO phase bin was normalized by dividing by the sum across all bins. Shown are fitted von Mises distributions to the binned, normalized amplitude. **C**, The preferred SO phase of low-gamma and high-gamma rhythms during sedation (mean ± SD across 10 sedated sessions) and of the high-gamma rhythm during sleep (mean ± SD across 4 sleep sessions).

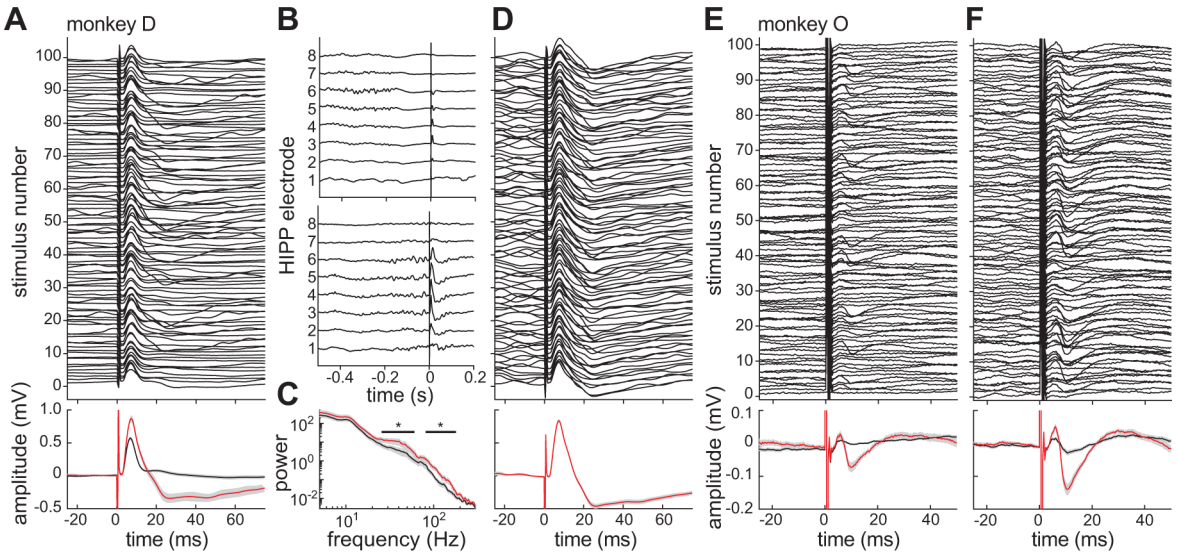

Figure 6.

State-dependent PHG-HIPP connectivity during sedation. **A**, Peri-stimulus HIPP responses to 100 PHG stimulus pulses in monkey D (top). Note the presence of a large, biphasic EP after a minority of stimuli. At the bottom, mean responses are shown for trials with (red) and without (black) a biphasic EP as determined by cluster analysis. 95% confidence intervals on the mean are shown in gray. **B**, Example raw recordings from all 8 electrodes on the HIPP array during two of the PHG stimulus trials shown in A. **C**, Mean power spectra of activity in the 300-ms window preceding the stimuli for the large-EP (red) and small-EP (black) trial clusters. The black lines indicate frequencies at with the power significant differed between the two groups. **D**, Peri-stimulus responses as in A but for a closed-loop experiment in which PHG stimulus pulses were triggered by high 30–50 Hz power in the HIPP recording. **E**, Results of same open-loop stimulation experiment as in A but conducted in monkey O. **F**, Results of closed-loop stimulation experiment in monkey O using 70–100 Hz power to trigger the stimuli.

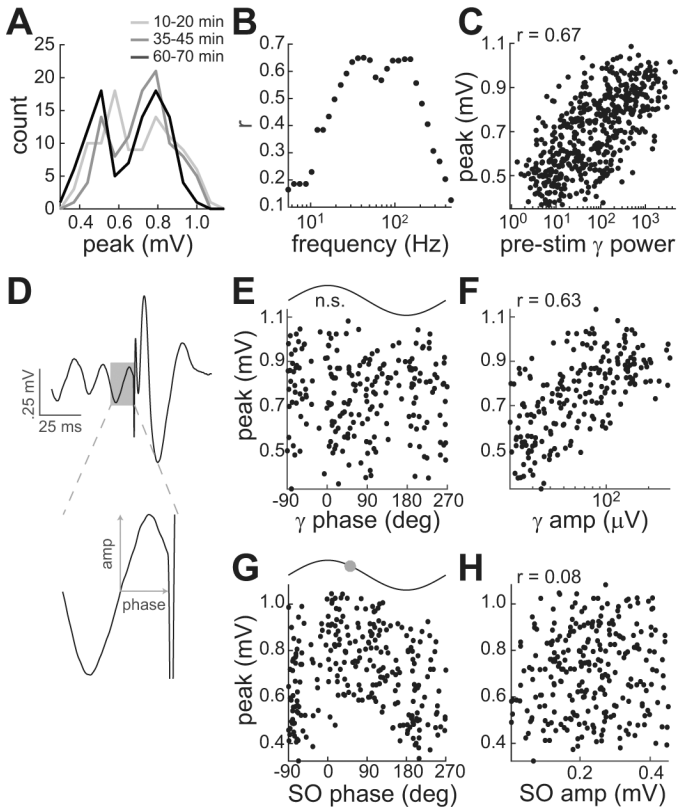

Figure 7.

Gamma and SO correlations with connectivity strength during sedation. Results are from a session with monkey D in which HIPP responses to 500 PHG stimuli were recorded. **A**, Bimodal distribution of peak EP values at the beginning, middle, and end of the session. **B**, Pearson's correlation coefficient (r) between EP peak and pre-stimulus power as a function of the frequency band in which power was calculated. For all bands, power was calculated in a 300-ms window preceding the stimulus. **C**, EP peak versus power in the band with maximum correlation (39–46 Hz). **D**, Example measurement of amplitude and phase of the oscillatory cycle immediately preceding the stimulus. Pre-stimulus gamma cycles were isolated by highpass filtering at 25 Hz (210 of 500 cycles preceding stimuli were within the 30–100 Hz range). Pre-stimulus SO cycles were isolated by lowpass filtering at 3 Hz (263 of 500 within the 0.5–2 Hz range). The measurements were used to quantify the relationship between EP peak and gamma phase (**E**), gamma amplitude (**F**), SO phase (**G**), and SO amplitude (**H**). For phase relationships with significant unimodal tuning, the preferred phase is indicated by the circle on the sine wave above the plot.

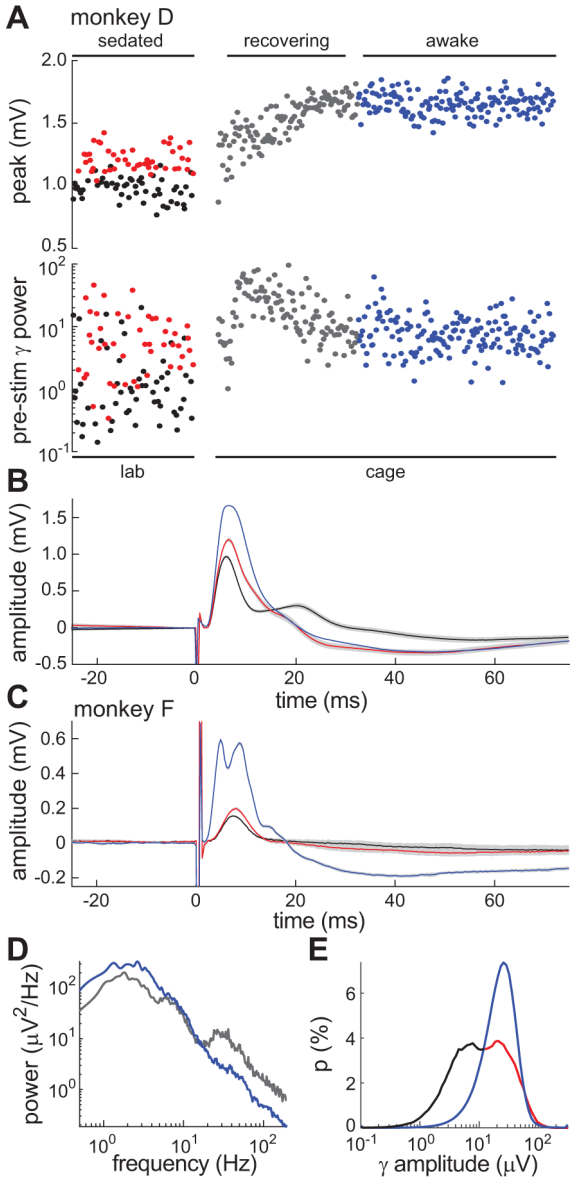

Figure 8.

Gamma-dependence of hippocampal EPs in sedated versus awake animals. **A**, Time course of EP peaks and pre-stimulus gamma power in monkey D across three behavioral states: sedated (red, black circles), recovery (gray circles), and awake (blue circles). Gamma (30–50 Hz) power was calculated in a 300-ms window preceding each stimulus. The horizontal axis is scaled to stimulus number not absolute time. PHG stimuli during sedation in the lab were delivered every 5 s by a commercial stimulator. PHG stimuli during recovery and awake periods in the home cage were delivered every 30 s by a custom wearable stimulator. Stimulus amplitude was 0.5 mA in both cases. The reversal agent, atipamezole, was given between the sedated and recovering states. **B**, Mean EPs during sedation (red, black) and awake (blue) for same dataset as A. 95% confidence intervals on the mean are shown in gray. **C**, Mean EPs for a sedated session (red and black) and awake session (blue) in monkey F. **D**, Power spectral density of the hippocampal recordings during recovery (gray) and

awake (blue) states in monkey F. **E**, Distribution of gamma amplitude across sedated (red, black) and awake (blue) recording sessions in monkey F. The sedated distribution was colored black and red to highlight its bimodal nature and correspondence to the bimodal EP response amplitudes of A-C.